actuators

MDPI

Article

A Positioning and Tracking Performance–Enhanced Composite Control Algorithm for the Macro–Micro Precision Stage

Zhiwei Zhou [1], Jian Gao [1,2] and Lanyu Zhang [1,2,*]

[1] State Key Laboratory of Precision Electronic Manufacturing Technology and Equipment, Guangdong University of Technology, Guangzhou 510006, China; 1112001002@mail2.gdut.edu.cn (Z.Z.); gaojian@gdut.edu.cn (J.G.)
[2] Key Laboratory of Intelligent Inspection and Manufacturing IoT of Ministry of Education, Guangdong University of Technology, Guangzhou 510006, China
* Correspondence: lanyuzhang@gdut.edu.cn

Abstract: In the macro–micro composite motion process, the macro stage achieves rapid motion in a large workspace, while the micro stage realizes precise positioning within a small displacement. The large-stroke and high-speed motion of the macro stage is influenced by nonlinear friction, overshooting, and vibrations, making it challenging to achieve rapid stabilization within the travel range of the micro stage, thereby impacting equipment operation efficiency. This paper proposes a composite controller structure designed to solve the fast point-to-point positioning of the macro stage driven by a linear motor and enhance the trajectory tracking performance of the stage. The proposed composite control algorithm (CCA) includes velocity feed-forward, gain-scheduled proportional integral differential (PID) control, and a plug-in repetitive control method. By employing a tracking differentiator, velocity feed-forward, and a gain-scheduled PID controller, the control algorithm can realize rapid stabilization and positioning for the macro stage. Through velocity feed-forward, gain-scheduled PID control, and a plug-in repetitive controller, the control algorithm can reduce the trajectory tracking error of the stage. Simulations and experimental studies of point response and sinusoidal trajectory tracking are carried out on a macro–micro stage to verify the effectiveness of the composite controller for the linear motor. The experimental results demonstrate that the proposed composite controller effectively reduces the macro stage's settling time and overshoot, and improves the accuracy of sinusoidal trajectory tracking, which lays a foundation for submicron positioning accuracy in high-speed macro–micro motion stages.

Keywords: macro–micro stage; precision positioning; trajectory tracking; composite control algorithm (CCA)

check for updates

Citation: Zhou, Z.; Gao, J.; Zhang, L. A Positioning and Tracking Performance–Enhanced Composite Control Algorithm for the Macro–Micro Precision Stage. *Actuators* **2024**, *13*, 433. https://doi.org/10.3390/act13110433

Academic Editor: Jose Luis Sanchez-Rojas

Received: 28 September 2024
Revised: 23 October 2024
Accepted: 25 October 2024
Published: 27 October 2024

Copyright: © 2024 by the authors. Licensee MDPI, Basel, Switzerland. This article is an open access article distributed under the terms and conditions of the Creative Commons Attribution (CC BY) license (https://creativecommons.org/licenses/by/4.0/).

1. Introduction

In the structural configuration of the macro–micro dual-stage driven motion stage, the macro stage performs rapid movements within a large workspace and achieves micro-level motion precision [1–3]. Simultaneously, the micro stage compensates precisely within a small displacement range [4,5]. This necessitates the rapid stabilization of the macro stage within the travel range of the micro stage; otherwise, achieving precise motion compensation by the micro stage becomes challenging. Therefore, the precise control of the macro stage is crucial for enhancing the overall control performance of the macro–micro composite precision stage [6–9]. The linear motor, serving as the macro stage's direct drive unit, exhibits high-speed and large-stroke motion characteristics. It has found extensive applications in advanced equipment manufacturing sectors such as integrated circuit fabrication, ultra-precision laser cutting, robotics, and automated inspection equipment [10–13].

However, the linear motor of the macro stage exhibits nonlinear friction issues during motion, impacting the dynamic performance of the motor's mover and drive components, thereby diminishing the macro stage's point-to-point positioning and trajectory tracking

performance [14–16]. In addressing the point-to-point positioning issue of the macro stage, numerous scholars have proposed control methods based on error feedback to enhance system positioning performance. For instance, Shin and Park [17] introduced an improved PID control method considering output saturation. This approach predicts the controller parameters during output saturation and dynamically updates the initial values within the linear region to reduce overshoot and positioning errors. Wu et al. [18] proposed a point-to-point positioning control method considering non-repetitive motion. This method utilizes a finite pulse response filter and sliding mode control to eliminate nonlinear friction, reducing the buffer positioning time and positioning error during motion state transitions. Tang et al. [19] presented a repetitive compensatory PID control method, effectively improving system positioning performance and reducing stabilization time. Zhang et al. [20] introduced a dynamic positioning method for rapidly decreasing stabilization time. The stage stabilization time decreased by 34.9% under a 40 mm stroke and 0.2 m/s velocity by initiating the motor at a specific moment and providing an appropriate control quantity. Song et al. [21] proposed a multi-objective optimization method based on a target function. This method uses finite element analysis data and regression calculations to learn the thrust distribution of the linear motor at different motion speeds, obtaining optimal control parameters for the linear motor and enhancing system positioning accuracy. Delibas et al. [22] proposed a novel positioning control method based on dual driving sources, which synchronizes the difference between the servo sampling frequency and the excitation frequencies of these sources to achieve stable motion and precise control at low speeds. Zheng et al. [23] proposed a comprehensive control strategy that combines a disturbance observer with H-infinity control, and achieved rapid and precise positioning of the recording head in hard disk drive systems. However, the error in the aforementioned feedback-based control methods is susceptible to noise amplification due to inaccuracies in differential signal acquisition. Moreover, these methods primarily focus on positioning accuracy after large-stroke point-to-point movements have reached their destination.

In addition to control methods developed for point-to-point positioning, Radac et al. [24] have suggested enhancing research on controllers applicable to precise motion trajectory tracking in the system. Such controllers are often designed using modern control theories and methods based on the system's internal mechanisms. Cui et al. [25] proposed an iterative learning control method based on wavelet transformation. This method reconstructs the error through wavelet coefficients and iteratively learns repeatable and non-repeatable errors, addressing the amplification issues of periodic and non-repeatable disturbances. Experimental results demonstrate that the wavelet iterative learning control method can effectively suppress non-periodic disturbances and improve the tracking performance of the system during multi-point movements. Liu et al. [26] introduced a model-based robust control method. This method effectively handles saturated nonlinearities and unmodeled dynamics through internal model and anti-saturation control, achieving high-precision stage tracking. Yang et al. [27] proposed an integrated control method combining a hysteresis compensator, input shaper, and high-gain feedback controller. This method eliminates hysteresis nonlinearity through inverse compensation using the actual model and suppresses vibration using input shaping and Smith predictive control. Experimental results show that the proposed method reduces tracking errors while addressing mild damping resonance issues. Wang et al. [28] presented a synchronous control method based on synchronous error models and state observers. This method estimates system states and external disturbances through a state observer and designs a synchronous controller using synchronous error models. It effectively reduces synchronization errors and tracking errors in multi-motor-driven stages, achieving position synchronization and disturbance suppression for each motor. Li et al. [29] proposed a repeat control method based on odd harmonic compensation. This method enhances system robustness through a low-pass filter and repeat control gain, introducing sensitivity functions to characterize system performance. It achieves precise position tracking of triangular wave trajectories. The control algorithms mentioned above primarily focus on the motion-tracking accuracy throughout

the entire motion process of the system, with less emphasis on positioning accuracy after the stage has reached its destination. This issue becomes increasingly important with the demand for improved precision in manufacturing equipment performance. For instance, in manufacturing microelectronic packaging equipment, the multi-level 3D interconnection process not only requires rapid and precise positioning under high dynamic conditions but also demands strict accuracy in line and arc trajectory formation. Ensuring that the stage maintains excellent motion-tracking accuracy is crucial for tracking desired motion curves [30–34].

Based on the comprehensive analysis, the precise control of the macro stage provides the conditions for the accurate compensation of the micro stage. Simultaneously, the control performance of the macro stage plays a crucial role in the overall performance of the macro–micro precision stage. With the increasing demand for narrow spacing, high-density chips, and device packaging equipment, the precision manufacturing field urgently requires a precision servo system with higher performance in motion accuracy, dynamic response, and settling time [35,36]. As one of the core components of electronic packaging equipment, the macro stage's positional movement and trajectory tracking control performance are directly related to the quality and efficiency of electronic manufacturing equipment. However, most of the current methods predominantly verify only positioning or tracking performance, making it difficult to meet the comprehensive performance requirements for stable positioning and trajectory tracking. Therefore, addressing the nonlinear friction issues in the motion process of the macro stage, a composite controller structure is proposed for point-to-point positioning and trajectory tracking control of the macro stage. The proposed composite control algorithm (CCA) includes velocity feed-forward, gain-scheduled PID control, and a plug-in repetitive control strategy. By employing a tracking differentiator, velocity feed-forward, and a gain-scheduled PID controller, the control algorithm can realize rapid stabilization and positioning for the macro stage. Through the velocity feed-forward, gain-scheduled PID control, and plug-in repetitive controller, the control algorithm can reduce the trajectory tracking error of the stage. Furthermore, to reduce the complexity of the composite controller, a study on dynamic modeling and model reduction is conducted by treating the linear motor mover, micro stage, and their connecting parts as a holistic entity. Parameter identification is performed to determine the reduced transfer function of the macro stage. In contrast to the previously mentioned control methods, the proposed composite controller is applied for precision positioning and sinusoidal trajectory tracking control of the macro stage. Currently, there is limited literature reporting on control methods and experimental results simultaneously improving both the point-to-point positioning and trajectory tracking performance of linear motors.

The summarized research contributions of this paper are as follows:

(1) Proposed a CCA method for the macro stage, including velocity feed-forward, gain-scheduled PID control, and a plug-in repetitive controller.
(2) The proposed controller can reduce the settling time and overshoot of the positioning process, and improve the trajectory tracking accuracy for the macro–micro stage with high positioning accuracy.

The remaining sections of this paper are organized as follows: Section 2 introduces the overall structure of the macro–micro precision stage, the dynamic modeling of the macro stage, and an analysis of model reduction. Section 3 conducts parameter identification for the reduced-order model. Section 4 elaborates on the CCA method. Section 5 performs a simulation analysis of the proposed CCA method. Section 6 involves the setup of the experimental apparatus for the macro–micro precision stage and experimental validation of the proposed CCA method. Finally, Section 7 summarizes the research findings of this work.

2. Modeling of the Macro Stage

2.1. Description of the Macro–Micro Precision Stage Structure

The overall structure of the macro–micro precision stage is illustrated in Figure 1. It primarily consists of an isolation base, precision guide rail, absolute grating scale, readout head, linear motor, and micro stage. The linear motor mover and the micro-stage are connected using a pre-tensioned spring structure, consolidating the linear motor mover, the micro stage, and the connecting part into a unified precision stage. The linear motor drives the integrated stage to achieve large-stroke precision positioning and high-precision trajectory tracking. A grating scale readout head measures the linear motor's motion displacement. The grating scale has a resolution of 1 nm, meeting the precision control requirements for position feedback during the macro stage's precise control.

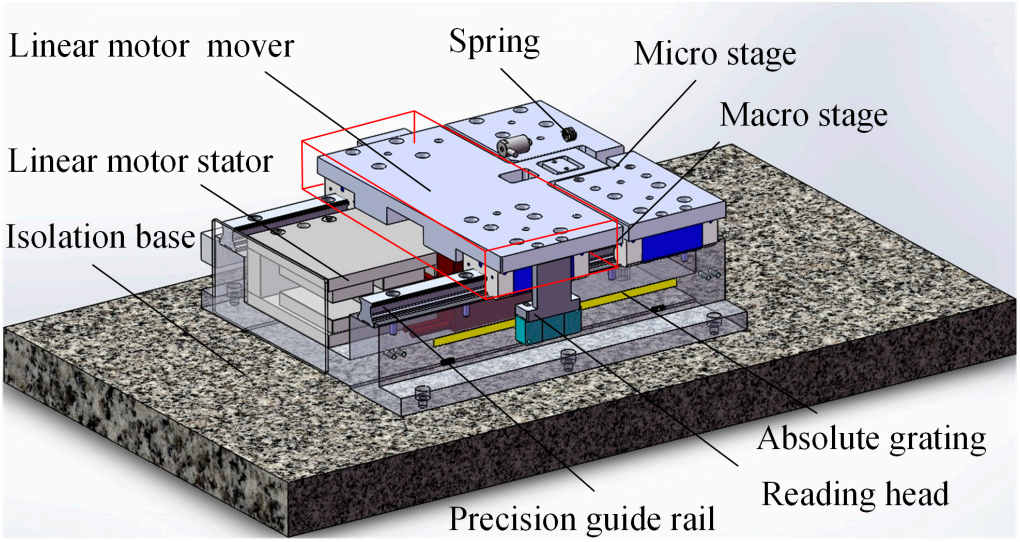


Figure 1. Structure of the macro–micro precision stage.

The piezoelectric ceramic element in the micro stage structure is mounted at the end position of the macro stage. A preloaded spring mechanism ensures firm contact between the output surface of the piezoelectric ceramic and the micro stage, allowing the micro stage to follow the macro stage's motion passively. During high-precision positioning, the piezoelectric ceramic adjusts its extension or contraction based on the displacement error, driving the micro stage and compressing the spring to achieve precise position compensation. The piezoelectric ceramic element provides high displacement precision, large output force, and fast response, enabling high-frequency operations with precise output control. Therefore, the integration of the piezoelectric ceramic with the preloaded spring mechanism facilitates rapid micro-compensation positioning, enhancing the overall performance of the macro–micro motion system. Specifically, the macro and micro motors are the AUM5-S1 model from Akribis and the PST150/7/7VS12 model from CoreMorrow, respectively.

2.2. Dynamic Modeling of the Macro Stage

Based on the structural description of the stage mentioned above, the overall dynamic model of the macro–micro precision stage is illustrated in Figure 2.

According to Newton's theorem and the motion process of the stage, the overall dynamic equations of the macro–micro precision stage can be expressed as follows:

$$\begin{cases} m_1\ddot{x}_1 = f_1 - k_1x_1 - c_1\dot{x}_1 - k_2(x_1 - x_2) - c_2(\dot{x}_1 - \dot{x}_2) - \mu\dot{x}_1 \\ m_2\ddot{x}_2 = f_2 - k_2(x_2 - x_1) - c_2(\dot{x}_2 - \dot{x}_1) - \mu\dot{x}_2 \end{cases} \tag{1}$$

where m_1, k_1, c_1, x_1, and f_1 are the equivalent mass, stiffness, damping coefficient, displacement, and electromagnetic thrust of the macro stage, respectively. k_2 and c_2 are the equivalent stiffness and damping coefficient of the connecting part between the linear motor mover and the micro stage, respectively. m_2 is the equivalent mass, including the micro stage and the connecting part. x_2 and f_2 are the displacement and driving force of the micro stage, respectively. μ is the contact-damping coefficient between the macro stage, micro stage, and guide rail.

Taking the Laplace transform of Equation (1) yields the following:

$$\begin{bmatrix} m_1s^2 + (c_1 + c_2 + \mu)s + k_1 + k_2 & -c_2s - k_2 \\ -c_2s - k_2 & m_2s^2 + (c_2 + \mu)s + k_2 \end{bmatrix} \begin{bmatrix} x_1(s) \\ x_2(s) \end{bmatrix} = \begin{bmatrix} f_1(s) \\ f_1(s) \end{bmatrix} \tag{2}$$

From Equation (2), the motion displacement of the linear motor is expressed as follows:

$$x_1(s) = D_{11}(s)f_1(s) + D_{12}(s)f_2(s) \tag{3}$$

where

$$D(s) = \begin{bmatrix} m_1s^2 + (c_1 + c_2 + \mu)s + k_1 + k_2 & -c_2s - k_2 \\ -c_2s - k_2 & m_2s^2 + (c_2 + \mu)s + k_2 \end{bmatrix}^{-1} = \begin{bmatrix} D_{11} & D_{12} \\ D_{21} & D_{22} \end{bmatrix} \tag{4}$$

To determine the transfer function of the macro stage, a staggered start-up approach is employed where the piezoelectric actuator on the micro stage remains inactive when the macro stage is in high-speed motion. Additionally, considering the rapid dynamic response of the current loop, with its control bandwidth significantly exceeding that of the position loop, the current loop is equivalently represented as a proportional link, as follows:

$$i_q(s) = \frac{3}{4}u_A(s) \tag{5}$$

where i_q and u_A are the q-axis current and voltage control signals of the linear motor, respectively.

According to the vector control method with i_d = 0, the relationship between the electromagnetic thrust of the motor and the q-axis current is expressed as follows:

$$f_1 = k_f i_q \tag{6}$$

where k_f is the motor thrust coefficient.

Therefore, substituting Equations (5) and (6) into Equation (3), the transfer function from the voltage control signal to the motion displacement of the macro stage is expressed as follows:

$$\frac{x_1(s)}{U_A(s)} = \frac{3(m_2s^2 + c_2s + k_2)k_f}{4[m_1s^2 + (c_1 + c_2 + \mu)s + k_1 + k_2](m_2s^2 + (c_2 + \mu)s + k_2) - 4(c_2s + k_2)^2} \tag{7}$$

From Equation (7), it can be observed that the macro stage is a fourth-order system. Typically, high-order systems complicate the design of controllers. Therefore, further reducing the model's order is necessary for the convenience of macro stage controller development.

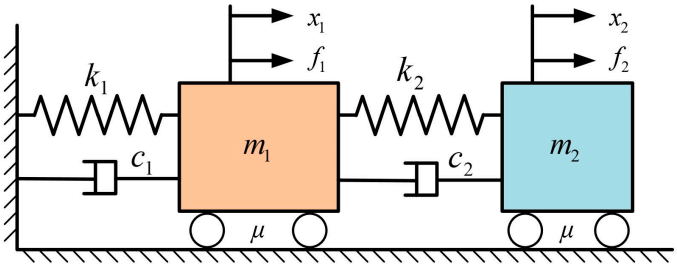


Figure 2. Overall dynamic model of the macro–micro precision stage.

2.3. Model Order Reduction Analysis

From Equation (2), the matrix form of the stage transfer function is further simplified as follows:

$$\begin{bmatrix} x_1(s) \\ x_2(s) \end{bmatrix} = \begin{bmatrix} \frac{1}{m_1 s^2 + (c_1 + c_2 + \mu)s + k_1 + k_2} & \frac{1}{c_2 s + k_2} \\ 0 & \frac{1}{m_2 s^2 + (c_2 + \mu)s + k_2} \end{bmatrix} \begin{bmatrix} f_1(s) \\ f_2(s) \end{bmatrix} \tag{8}$$

From Equation (8), the coupled motion relationship between the macro stage and the micro stage is expressed as follows:

$$\hat{x}_1(s) = \frac{1}{c_2 s + k_2} f_2(s) \tag{9}$$

where $\hat{x}_1$ is the coupled displacement.

Taking the inverse Laplace transform of Equation (9) yields the following:

$$\hat{x}_1 = \frac{1}{c_2} e^{-\frac{k_2}{c_2} t} f_2 \tag{10}$$

When the equivalent stiffness, k_2, of the connecting part is set to a relatively large value, we can obtain

$$\frac{k_2}{c_2} \to \infty \tag{11}$$

Therefore, the coupled displacement, $\hat{x}_1$, between the macro and the micro stages tends to be zero.

Substituting Equations (10) and (11) into Equation (7), the transfer function of the macro stage is simplified as follows:

$$G_n(s) = \frac{x_1(s)}{U_A(s)} = \frac{4k_f}{3m_1 s^2 + (c_1 + c_2 + \mu)s + 3(k_1 + k_2)} \tag{12}$$

3. Parameter Identification

According to the reduced-order model analysis shown in Equation (12), the macro stage can be considered as a second-order linear system. To obtain a more accurate linear model, this study uses a continuously varying sine signal as the excitation signal. The sweep frequency has an amplitude of 1 V, a frequency range of 1 Hz–500 Hz, and a sweep time of 10 s. In addition, the stage's excitation voltage and output displacement are collected through a dSPACE controller. The frequency response is obtained through a discrete Fourier transform, and data fitting is performed using the least squares method. Based on the open-loop frequency fitting curve, the transfer function of the macro stage is obtained and represented as follows:

$$G_n(s) = \frac{4683.3}{s^2 + 18.85s^2 + 61.68} \tag{13}$$

The comparison between the system identification and experimental test results is shown in Figure 3. It can be observed that the system identification model demonstrates a

good fit with the experimental test results at low frequencies, while there is uncertainty in the high-frequency range.

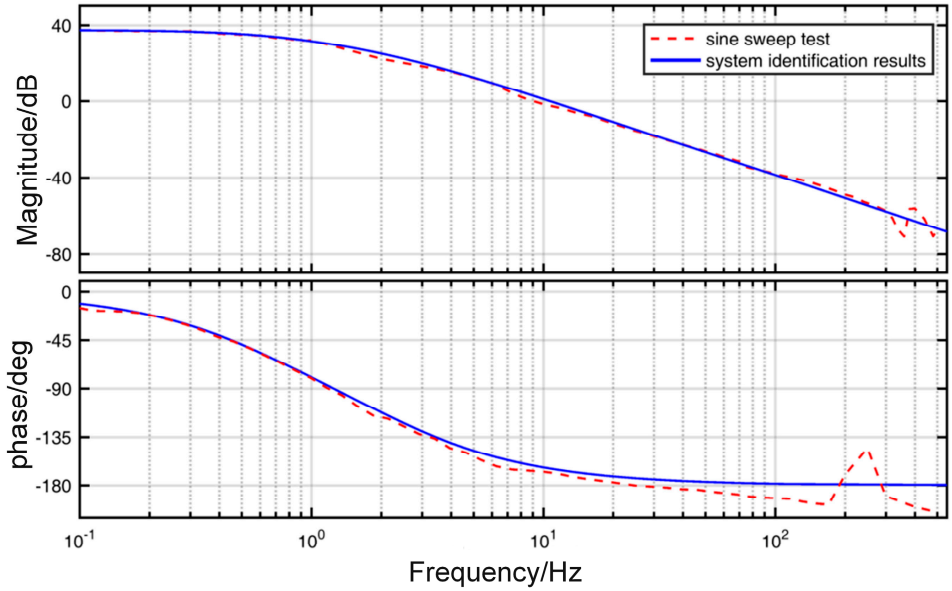


Figure 3. Comparison of system identification and experimental results.

4. CCA Control Schemes

Based on the above dynamic modeling and parameter identification analysis, a composite controller is designed for the macro stage's point-to-point positioning and trajectory tracking control. The following sections will describe the design of the positioning and trajectory tracking control modules.

4.1. Tracking Differentiator and Gain-Scheduled PID Control for Positioning

Point-to-point control aims to achieve high-precision positioning of the stage within a small settling time and overshoot. The composite control method includes velocity feed-forward and gain-scheduled PID feedback control, which is illustrated in Figure 4. In this approach, gain-scheduled PID control takes the displacement error as the control input and adjusts the servo gain through a scheduling function to mitigate the impact of nonlinear friction on positioning performance, enabling fast motion and positioning of the macro stage. The velocity feed-forward controller is employed to enhance the system's response speed. The tracking differentiator is used to smoothly approximate the originally planned trajectory, effectively estimate velocity, reduce noise amplification, and obtain a smooth differential signal.

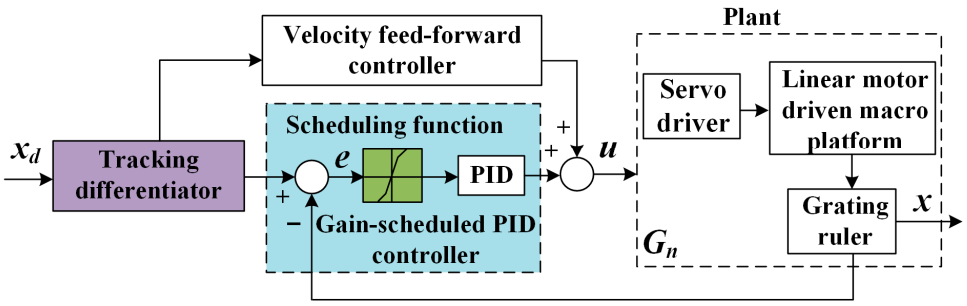


Figure 4. Control method for fast positioning.

The difference equation representation of the discretized first-order tracking differentiator is given as follows:

$$\begin{aligned} x_3(k+1) &= x_3(k) + T_s \cdot x_4(k) \\ x_4(k+1) &= x_4(k) + T_s \cdot fst_2(x_3(k) - x_d(k), x_4(k), r_0, T_s) \end{aligned} \tag{14}$$

where x_d is the desired trajectory, x_3 and x_4 are the tracking differentiator's state variables, T_s is the sampling period, and r_0 is the speed factor reflecting the tracking speed. According to the theory of optimal control, derive the optimal comprehensive control function $fst_2(\cdot)$, expressed as follows:

$$\begin{aligned} & d = T_s r_0, d_0 = T_s d, y = x_3 + T_s x_4 \\ & a_0 = \sqrt{d^2 + 8r_0|y|} \\ & a = \begin{cases} x_4 + \frac{a_0 - d}{2} sign(y), |y| > d_0 \\ x_4 + y/T_s, |y| \le d_0 \end{cases} \\ & fst_2(x_3, x_4, r_0, T_s) = \begin{cases} -r_0 sign(a), |a| > d \\ -r_0 \frac{a}{d}, |a| \le d \end{cases} \end{aligned} \tag{15}$$

Equation (15) represents the optimal control function synthesized using the equidistant zone method. This form of tracking differentiator exhibits excellent tracking performance and differentiation characteristics and eliminates oscillations. The tracking speed of this differentiator depends on the speed factor.

Next, a gain-scheduled PID controller is proposed to avoid instability during point-to-point positioning control of the macro stage based on the PID control structure. As the macro motion stage approaches the target point, the servo stiffness is dynamically adjusted in real time through servo gain adjustment. The basic principle of this controller involves setting a critical value for the gain-scheduled region and adjusting the servo gain using a scheduling coefficient to enhance the macro stage's fast and high-precision positioning performance. The gain-scheduled PID control structure is shown in Figure 5.

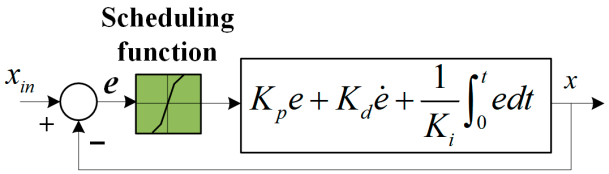


Figure 5. Gain scheduling PID control structure.

As shown in Figure 5, the output equation of the gain-scheduled PID controller is represented as follows:

$$u_{gspid} = K_{pgs}(K_p e + K_d \dot{e}) + \frac{1}{K_i}\int_0^t e dt \tag{16}$$

where e is the tracking error, K_p, K_i, and K_d are the proportional, integral, and derivative coefficients, respectively, and K_{pgs} is the gain scheduling function, with its control variable expressed as:

$$K_{pgs} = \begin{cases} \delta & |e| \le \varphi \\ 1 & |e| > \varphi \end{cases} \tag{17}$$

where φ is the critical value of the gain scheduling zone, and δ is the scheduling coefficient, which can be set between 0 and 5. Since setting δ to 1 does not change the system's stiffness, we set $\delta > 1$ to enhance servo stiffness and dynamic response capabilities.

The relationship between the error and the servo stiffness under the gain scheduling mechanism is illustrated in Figure 6. When $\delta > 1$, the gain K_{pgs} increases, indicating that the servo stiffness in the scheduling zone is greater than outside the scheduling zone, as

shown in the orange region in Figure 6. When $0 < \delta < 1$, the servo stiffness decreases, as depicted in the purple area in Figure 6. When the system operates outside the gain scheduling zone, i.e., when the error $e > \varphi$, the scheduling coefficient $\delta = 1$, and the gain K_{pgs} remains unchanged.

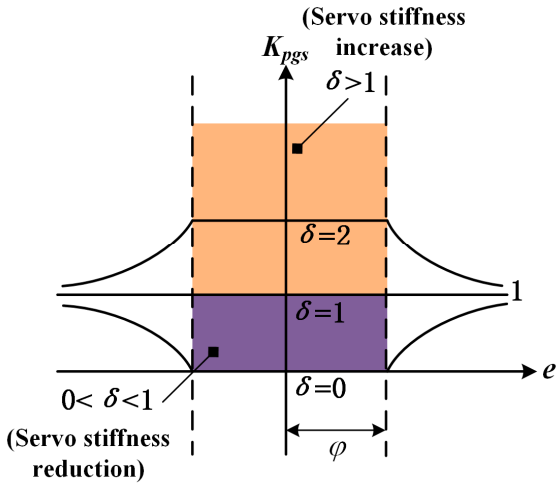


Figure 6. Relationship between error and servo stiffness in gain scheduling control.

4.2. Plug-In Repetitive Control for Trajectory Tracking

The purpose of trajectory tracking control is to enhance the control precision throughout the entire motion process of the system. Due to the relatively singular frequency components of the sine function and the ability to obtain various curves through the superposition of sine functions, this paper employs the sine function as the reference input for trajectory tracking control. The composite control method includes velocity feed-forward, gain-scheduled PID feedback, and repetitive control, as illustrated in Figure 7. Unlike the control structure in Figure 4, trajectory tracking control obtains the input signal for the velocity feed-forward controller through direct differentiation. The discrete-time repetitive controller here is designed as a plug-in feedback controller to track periodic reference signals accurately. The discrete-time repetitive control method is relatively straightforward to implement in practical applications, and the system's initial state does not need to be restored to the desired condition at each run.

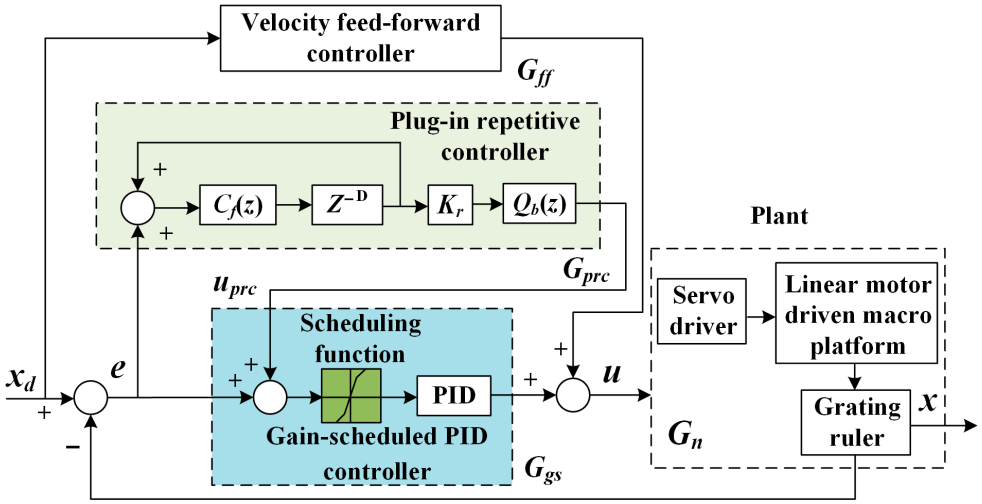


Figure 7. Control method for sinusoidal trajectory tracking.

As shown in Figure 7, the plug-in repetitive controller comprises a filter $C_f(z)$, repetitive control gain K_r, compensator $Q_b(z)$, and delay element Z^{-D}. D is the number of

samples per signal cycle, expressed as $D = T_r/T_s$, where T_r is the period of the reference input. The filter $C_f(z)$ is employed to enhance system robustness, the gain K_r balances system stability and tracking performance, and the compensator $Q_b(z)$ increases the closed-loop system bandwidth and further reduces tracking error, defined as $Q_b(z) = z^m$, where m is a positive constant. G_{ff}, G_{gs}, and G_n are the transfer functions of velocity feed-forward, gain-scheduled PID feedback, and the macro stage, respectively. The transfer function $G_{prc}(z)$ of the plug-in repetitive controller from e to u_{prc} can be expressed as follows:

$$G_{prc}(z) = \frac{u_{prc}(z)}{e(z)} = \frac{k_r Q_b(z) C_f(z) z^{-D}}{1 - C_f(z) z^{-D}} \tag{18}$$

Constructing the filter $C_f(z)$ in the RC control module can be represented as follows:

$$C_f(z) = \frac{\tau}{1 - z^{-1}(1 - \tau)} \tag{19}$$

where τ satisfies $0 < \tau < 1$, typically, due to the frequency characteristics of $C_f(z)$, it will reduce high-frequency gains. To enhance the robustness of the control system, this will affect the system's tracking accuracy. Therefore, when selecting $C_f(z)$, a trade-off between system robustness and tracking error should be considered.

The complementary sensitivity function $T_{oc}(z)$ with repetitive control in Figure 7 is expressed as follows:

$$T_{oc}(z) = \frac{x(z)}{x_d(z)} = \frac{\Big(\big(1 + G_{prc}(z)\big) G_{gs} + G_{ff}\Big) G_n}{1 + \big(1 + G_{prc}(z)\big) G_{gs} G_n} \tag{20}$$

Similarly, the complementary sensitivity function without repetitive control, $\hat{T}_{oc}$, is expressed as follows:

$$\hat{T}_{oc}(z) = \frac{\Big(G_{gs} + G_{ff}\Big) G_n}{1 + G_{gs} G_n} \tag{21}$$

Combining Equations (20) and (21), the corresponding sensitivity functions $S_{oc}(z)$ and $\hat{S}_{oc}$ are derived and expressed as follows:

$$\begin{cases} S_{oc}(z) = \frac{1}{1 + \big(1 + G_{prc}(z)\big) G_{gs} G_n} \\ \hat{S}_{oc}(z) = \frac{1}{1 + G_{gs} G_n} \end{cases} \tag{22}$$

From Equation (18), the expression of $S_{oc}(z)$ in Equation (22) can be rewritten as follows:

$$S_{oc}(z) = \hat{S}_{oc}(z) \cdot \frac{1 - C_f z^{-D}}{1 - C_f(z) z^{-D} \big(1 - \big(1 - \hat{S}_{oc}(z)\big) k_r Q_b(z)\big)} \tag{23}$$

Therefore, according to the small-gain theorem, assuming internal stability of the closed-loop system without repetitive control, for $D > 0$, the conditions for the internal stability of the control system used for sine trajectory tracking can be expressed as follows:

$$\| C_f\Big(e^{j\omega T_s}\Big) \Big(1 - \Big(1 - \hat{S}_{oc}\Big(e^{j\omega T_s}\Big)\Big) k_r Q_b\Big(e^{j\omega T_s}\Big)\Big) \| < 1, \text{ For all } 0 \le \omega < \pi/T_s \tag{24}$$

Equation (24) indicates that all poles of the system sensitivity function, $S_{oc}(z)$, are located within the unit circle of the complex plane.

5. Simulation Analysis

To verify the effectiveness of the composite controller, this section presents the control effects of the macro stage in point response and sinusoidal trajectory tracking with and

without the CCA method. The control method combining velocity feed-forward and PID feedback control is called the without CCA method.

5.1. Point Response Simulation

To ensure a fair comparison of control algorithms, optimal control parameters were selected for all controllers, with K_f, K_p, K_i, and K_d set to 0.000055, 85.572, 0.422, and 0.193, respectively. Additionally, r_0, T_s, φ, and δ were set to 1,000,000, 0.0001, 0.1, and 1.5, respectively. It is worth noting that the controller parameters for velocity feed-forward and PID feedback control remain constant during the simulation.

To verify the effects of the CCA method on the precision positioning of the macro stage, simulations were performed for an S-curve with a velocity of 0.1 m/s, acceleration of 10 m/s^2, and various amplitudes. Figure 8 and Table 1 show the CCA method's impact on the positioning performance of the macro stage. It can be observed that the proposed CCA method effectively reduces the overshoot and settling time of the macro stage. Specifically, compared to the control method without CCA, the proposed CCA method reduces the overshoot and settling time by 90.31% and 64.41%, respectively, at a 10 mm amplitude, thereby validating the effectiveness of the proposed controller.

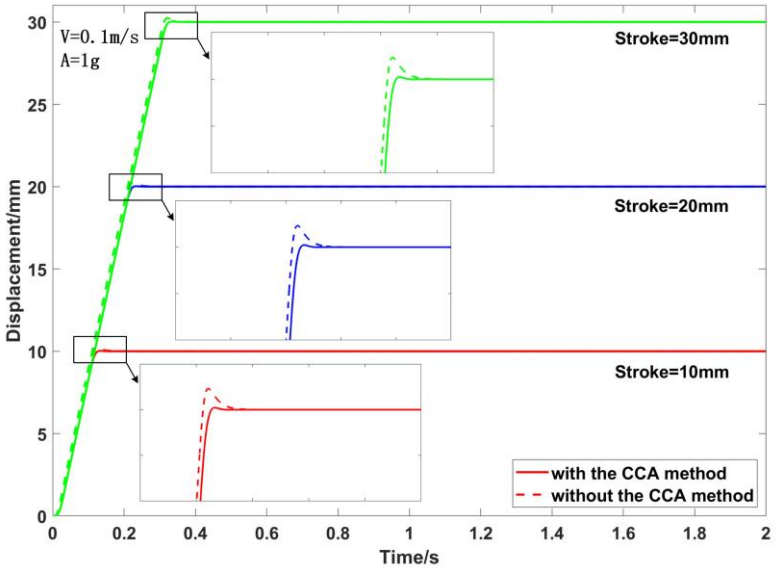


Figure 8. Displacement curves of point response with the CCA method.

Table 1. Comparison of positioning performance with the CCA method.

Motion Parameters			Overshoot (μm)			Settling Time (ms)		
Stroke (mm)	Velocity (m/s)	Acceleration (m/s^2)	Without CCA	With CCA	Reduction (%)	Without CCA	With CCA	Reduction (%)
10	0.1	10	232.01	22.47	90.31	85.13	30.29	64.41
20	0.1	10	232.33	22.98	90.11	85.18	30.63	64.04
30	0.1	10	232.33	22.99	90.10	85.23	30.66	64.02

5.2. Sinusoidal Trajectory Tracking Simulation

Like the point response control, the control parameters K_f, K_p, K_i, and K_d are set to 0.000055, 85.572, 0.422, and 0.193, respectively. Additionally, based on the performance analysis of the repetitive controller in Equation (24), τ, K_r, T_s, and m are set to 0.085, 0.95, 0.0001, and 100, respectively. To verify the effects of the CCA method on the tracking performance of the macro stage, a simulation analysis is conducted for a sinusoidal trajectory with a 5 mm amplitude and 1 Hz frequency. The simulation results for displacement and tracking error are shown in Figure 9. It can be seen from Figure 9 that, compared to the

control method without CCA, employing the CCA method allows for better tracking of the desired trajectory and reduces tracking error, achieving high-precision trajectory tracking control for the stage. Additionally, regarding the phase difference in the tracking error shown in Figure 9b, this is related to the delay in the repetitive control algorithm. This method enhances performance through learning, but it may introduce time delays during the process, resulting in phase shifts.

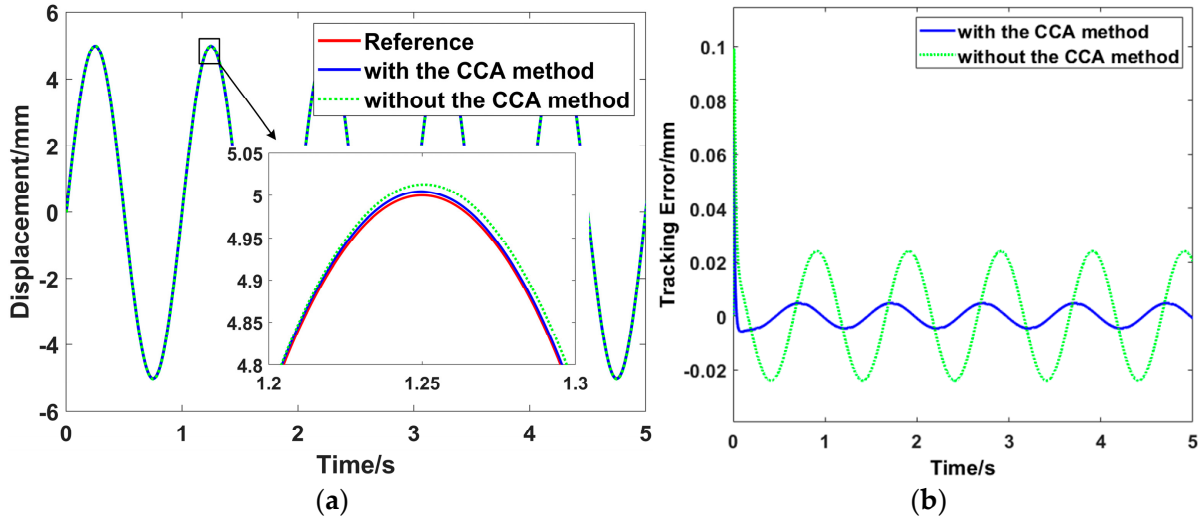


Figure 9. Displacement and tracking error of sinusoidal trajectory tracking with the CCA method at 5 mm amplitude and 1 Hz frequency. (**a**) Displacement, (**b**) Tracking error.

Additionally, to quantitatively analyze the effectiveness of the CCA method, the mean absolute error (MAE) and standard deviation (STD) are used as evaluation metrics for tracking errors. Figure 10 presents simulation results of sine trajectory tracking at a 10 mm amplitude and different frequencies with and without the CCA method, and the corresponding evaluation metrics are shown in Table 2. It can be observed that the proposed CCA method reduces the STD tracking error by 85% and 60.54% at frequencies of 0.1 Hz and 2 Hz, respectively, compared to the control method without CCA, thereby confirming the effectiveness of the proposed CCA method in trajectory tracking control.

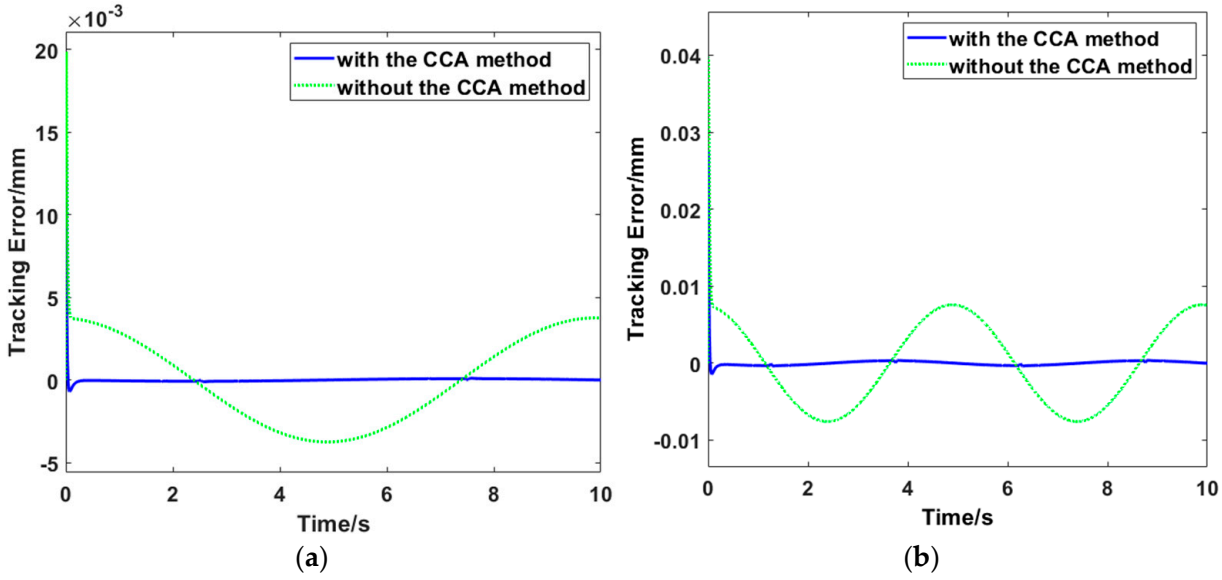


Figure 10. *Cont.*

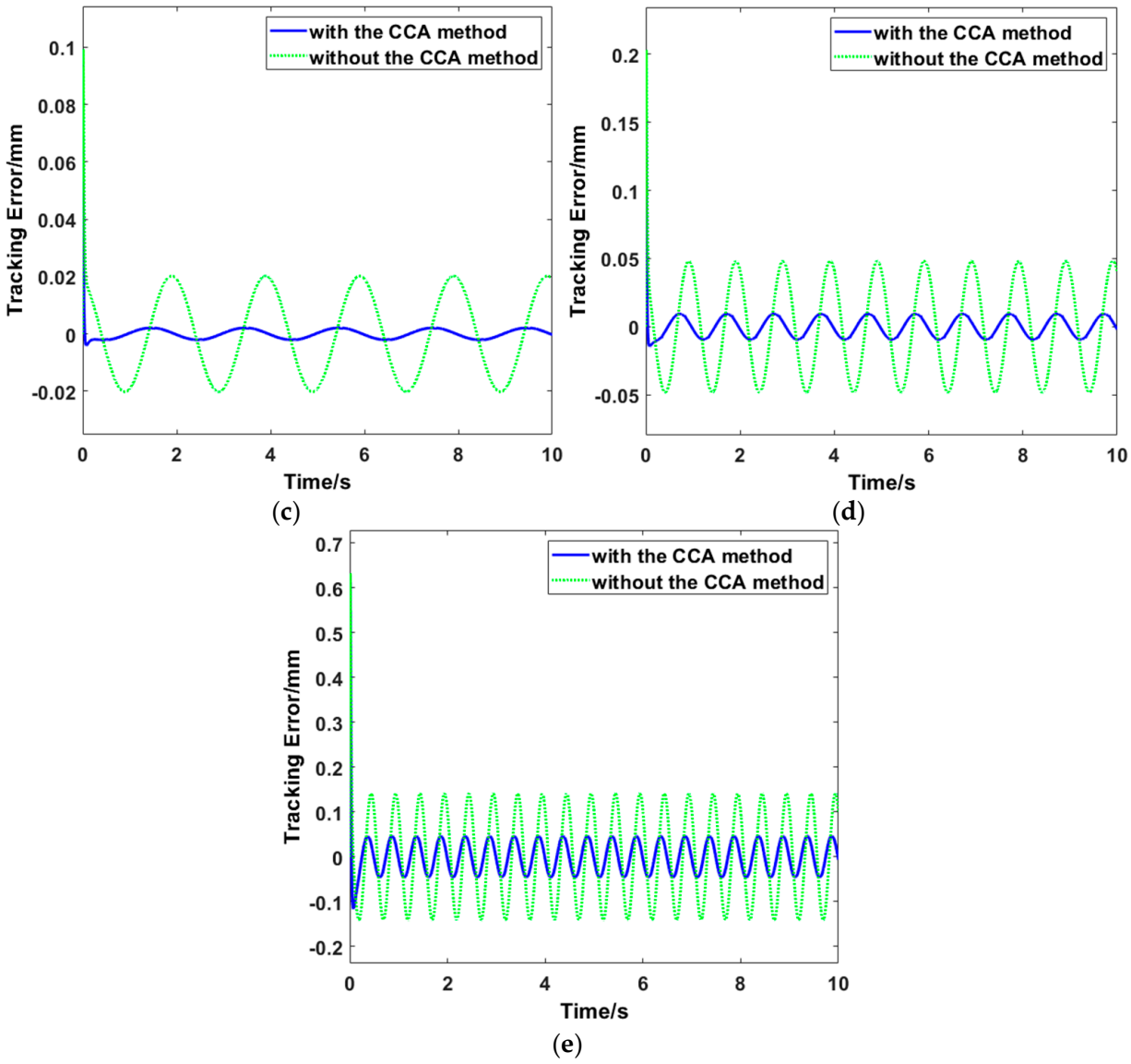


Figure 10. Tracking error with the CCA method at different frequencies. (**a**) 0.1 Hz, (**b**) 0.2 Hz, (**c**) 0.5 Hz, (**d**) 1 Hz, (**e**) 2 Hz.

Table 2. Comparison of performance indexes for sinusoidal trajectory tracking at different frequencies.

Sinusoidal Trajectory		Tracking Error (μm)				
Amplitude (mm)	Frequency (Hz)	Without the CCA		With the CCA		STD Reduction (%)
		MAE	STD	MAE	STD	
10	0.1	2.4	2.8	0.08	0.42	85.0
10	0.2	4.9	5.6	0.26	0.87	84.45
10	0.5	13.1	14.9	1.5	2.6	82.55
10	1	31.1	35.2	6.3	8.3	76.42
10	2	91.3	103.4	31.5	40.8	60.54

6. Experimental Verification

To validate the control performance of the composite controller, an experimental setup for the macro–micro stage was constructed, as illustrated in Figure 11. The structure comprises an upper computer, the macro stage, the micro stage, the dSPACE controller, and the Akribis ASD240-0418 servo driver module. The macro stage consists of a one-

dimensional guiding mechanism, linear motor, and high-resolution grating ruler. The AUM5-S1 series linear motor drives the guiding mechanism with a maximum displacement of 40 mm. The AK LIC411 grating ruler is employed to measure the real-time displacement of the macro stage with a feedback resolution of 1 nm. The dSPACE-DS2655 controller is utilized to implement the proposed CCA method. Additionally, the system sampling period T_s is set to 0.0001 s.

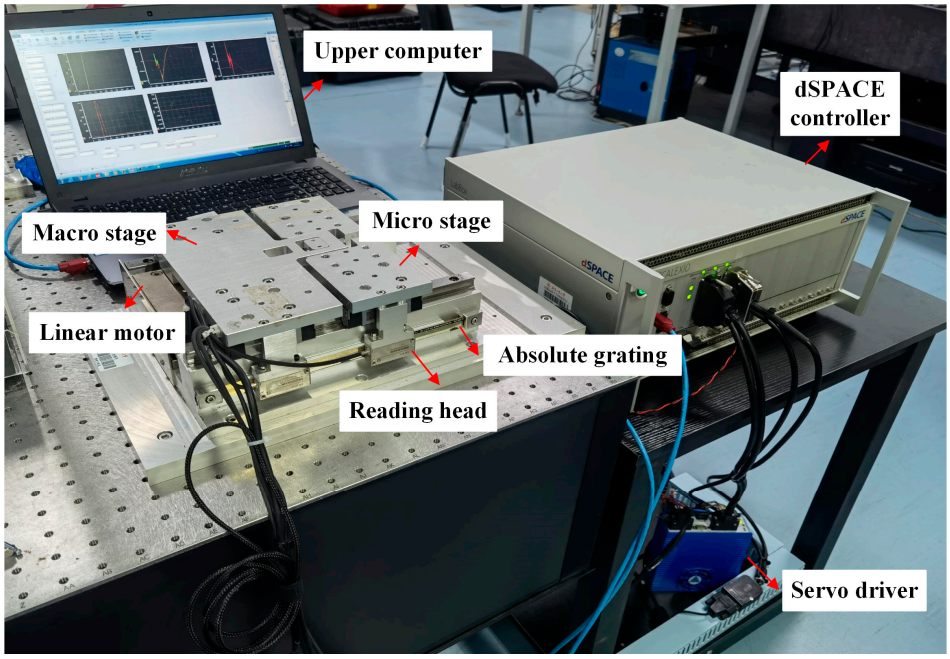


Figure 11. Experimental setup of the macro–micro precision stage.

6.1. Point Response Experiment

In the experimental process, an S-curve with a velocity of 0.1 m/s, acceleration of 10 m/s², and varying amplitudes was applied to the macro–micro stage. The control methods with and without CCA were implemented under the same conditions to achieve high-precision positioning while ensuring stage stability. The following steps were taken to tune the parameters of the proposed control method. Since the proposed controller is a development version of the method without CCA, the control parameters of the method without CCA were first optimized. Through experimental trial and error, the optimal control parameters were determined, ensuring high-precision positioning when the stage operates rapidly and stably. Given that the proposed controller incorporates additional auxiliary components based on the method without CCA, the parameters of the auxiliary components were determined through trial-and-error experiments while maintaining consistency with the original control parameters of the method without CCA. Thus, the optimal parameters for both methods, with and without CCA, were selected, with K_f, K_p, K_i, and K_d set to 1.96, 6000, 1000, and 7, respectively, and r_0, φ, and δ set to 1,000,000, 0.1, and 1.12, respectively.

Figure 12 and Table 3 illustrate the control effects of methods with and without CCA on the positioning performance of the macro stage. It can be seen that, compared to the method without CCA, the overshoot and settling time of the method with CCA reduced by 93.2% and 27.3%, respectively, under a 10 mm amplitude. Additionally, for the same macro stage, the settling time and overshoot of the control method that Liu et al. [37] proposed for 10 mm positioning are 243 ms and 35 μm, respectively, which are longer than those of the CCA method proposed in this paper. Therefore, the experimental results further validate the effectiveness and advancement of the proposed CCA method.

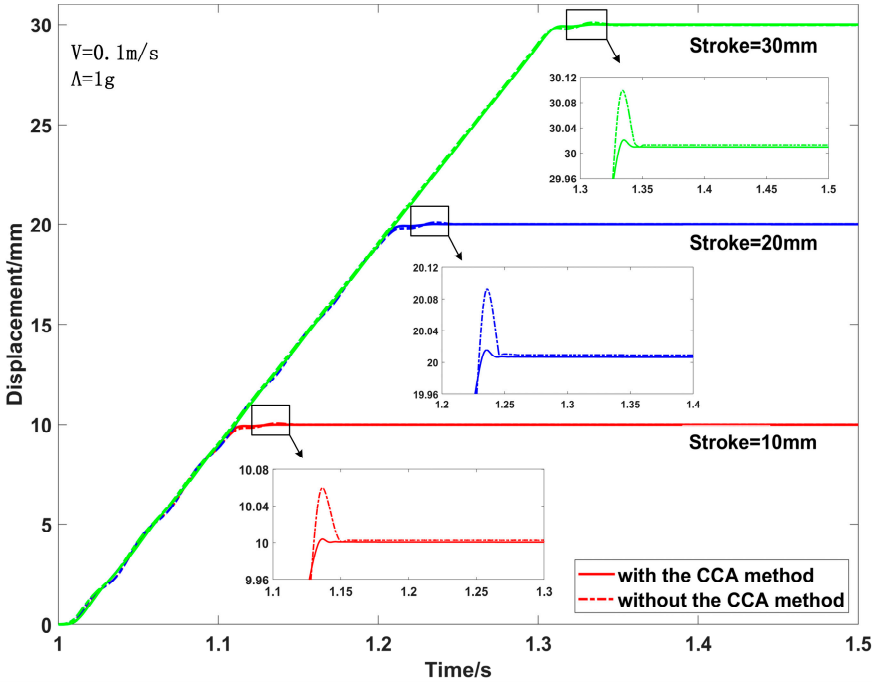


Figure 12. Experimental results of point response with the CCA method.

Table 3. Experimental comparison of positioning performance with the CCA method.

Motion Parameters			Overshoot (μm)			Settling Time (ms)		
Stroke (mm)	Velocity (m/s)	Acceleration (m/s^2)	Without CCA	With CCA	Reduction (%)	Without CCA	With CCA	Reduction (%)
10	0.1	10	59.7	4.0	93.2	36.6	26.6	27.3
20	0.1	10	82.3	15.1	81.6	39.8	31.1	21.8
30	0.1	10	91.1	21.5	76.4	45.1	35.8	20.6

6.2. Sinusoidal Trajectory Tracking Experiment

Similar to Figure 4, a feedback control system was implemented using a gain-scheduled PID control module, where K_f, K_p, K_i, and K_d were set to 0.000055, 2600, 2.5, and 26, respectively. Additionally, φ and δ were set to 0.1 and 1.002, respectively. Furthermore, τ was set to 0.085 to reduce the control gain of the plug-in repetitive controller in the high-frequency region. Experimental investigations determined K_r, T_s, and m to be 0.92, 0.0001, and 100, respectively. It is important to note that the tuning steps for the parameters of the proposed controller during the tracking experiments are the same as those for the aforementioned positioning experiments, and that the parameters of the designed repetitive controller should satisfy the stability condition in Equation (24).

The experiment utilized a sinusoidal trajectory with a 5 mm amplitude and 1 Hz frequency as the reference input. The results are presented in Figure 13. As evident from Figure 13, when employing the proposed CCA method, the actual output of the macro stage closely aligns with the reference input, leading to a rapid reduction in tracking error for the macro stage.

Figure 14 presents the experimental results for sinusoidal trajectory tracking with a 10 mm amplitude at varying frequencies. The specific evaluation metrics for tracking performance are detailed in Table 4. It can be observed that, compared to the control method without CCA, the proposed CCA method achieves reductions of 96.63% and 82.73% in STD tracking error at frequencies of 0.1 Hz and 2 Hz, respectively. This finding validates the effectiveness of the proposed CCA method in reducing tracking error across a wide frequency range.

Table 4. Experimental results of tracking performance with the CCA method at different frequencies.

Sinusoidal Trajectory		Tracking Error (μm)				
Amplitude (mm)	Frequency (Hz)	Without the CCA		With the CCA		STD Reduction (%)
		MAE	STD	MAE	STD	
10	0.1	138.2	142.5	2.5	4.8	96.63
10	0.2	136.3	141.7	3.6	7.4	94.77
10	0.5	120.9	124.5	5.3	10.9	91.24
10	1	106.9	110.3	7.3	13.8	87.48
10	2	104	129.2	16.3	22.3	82.73

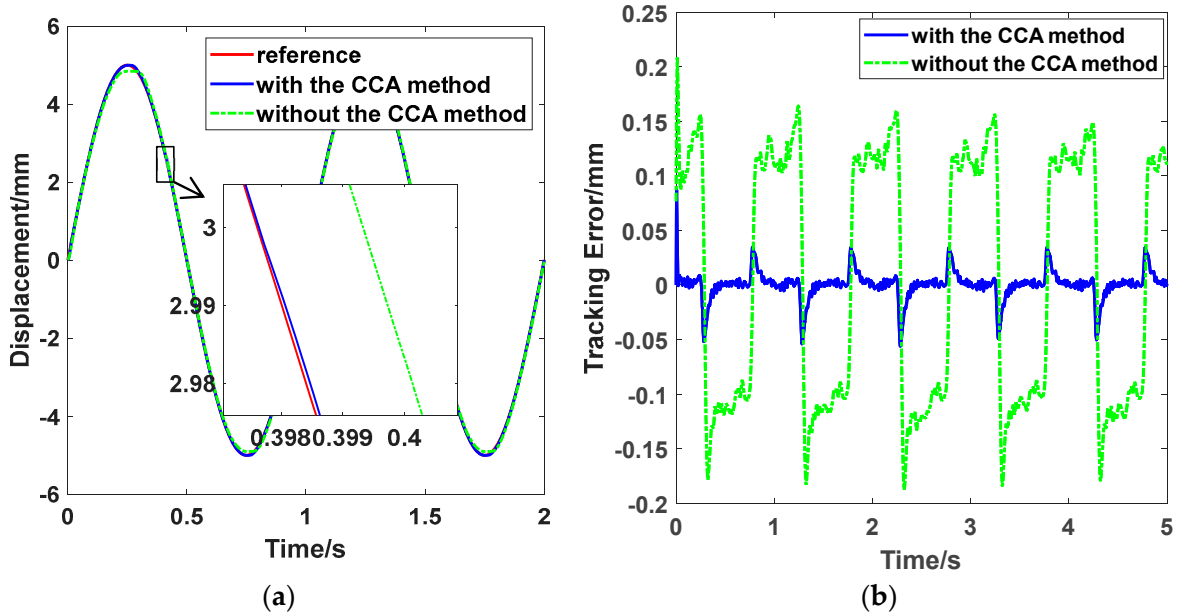


Figure 13. Experimental results for sinusoidal trajectory tracking with the CCA method at 5 mm amplitude and 1 Hz frequency. (**a**) Displacement, (**b**) Tracking error.

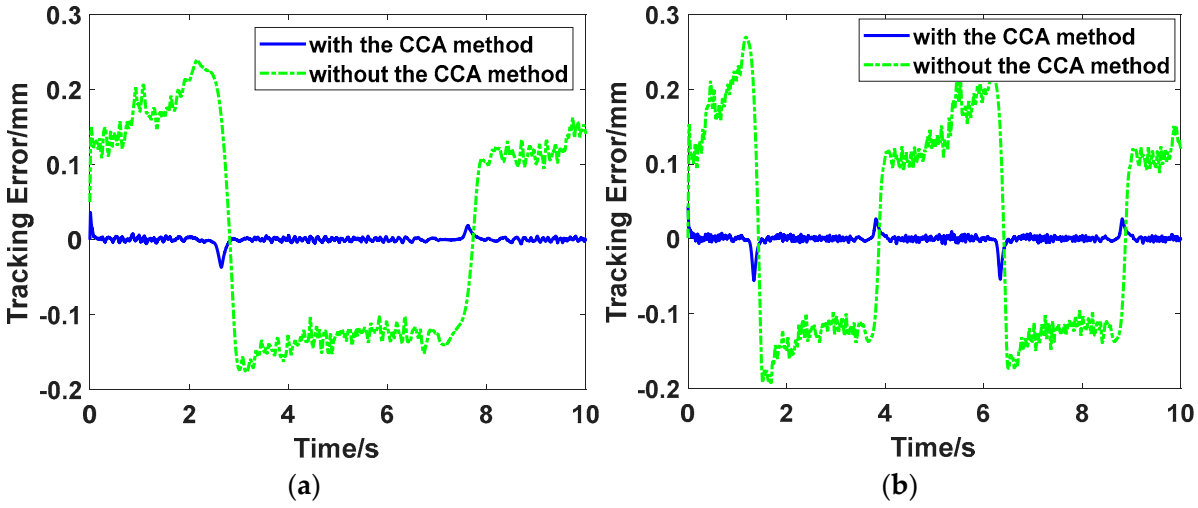


Figure 14. *Cont.*

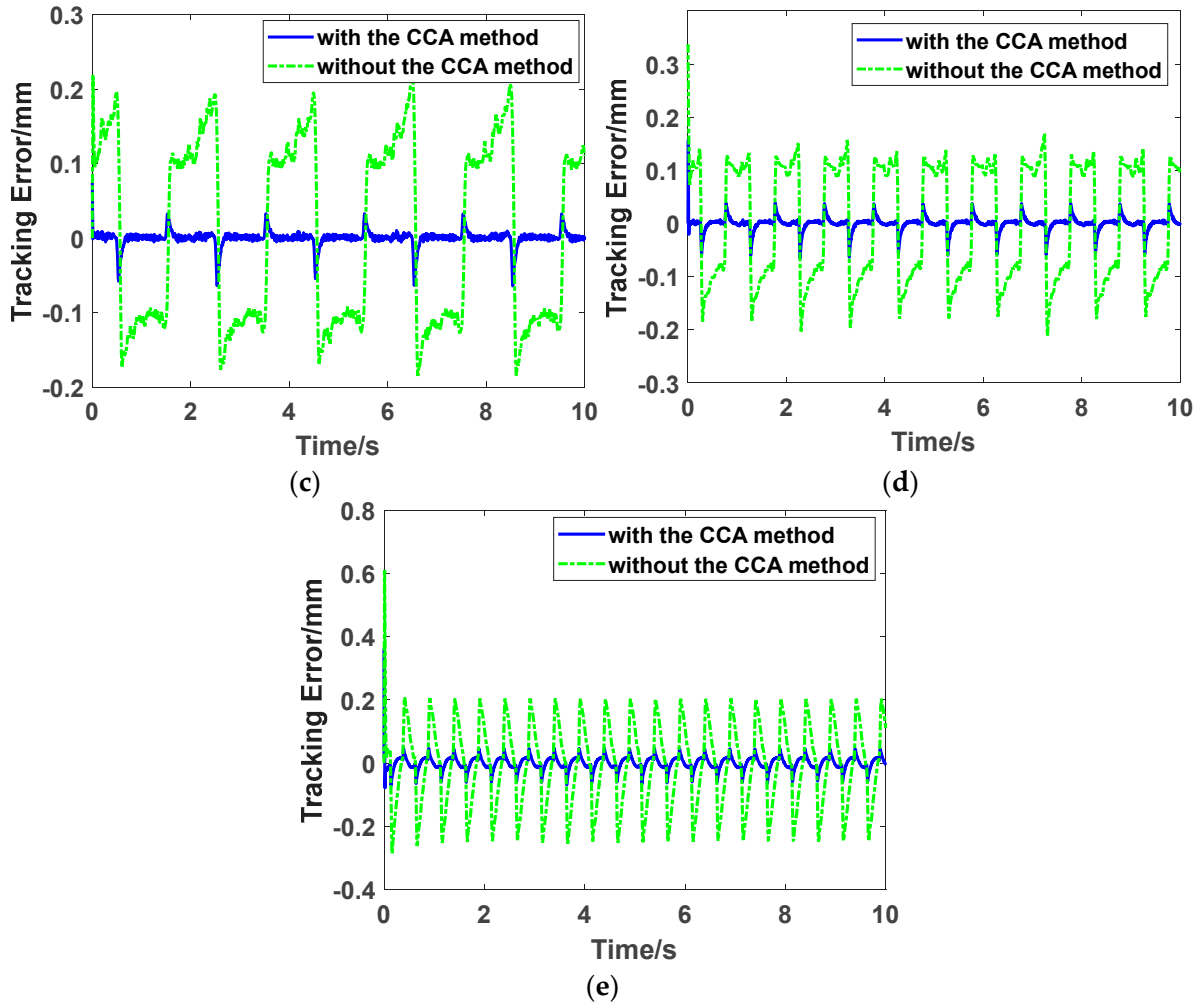


Figure 14. Experimental results of tracking error with the CCA method at different frequencies. (**a**) 0.1 Hz, (**b**) 0.2 Hz, (**c**) 0.5 Hz, (**d**) 1 Hz, (**e**) 2 Hz.

Finally, when contrasting the simulation outcomes presented in Tables 1–4 with the experimental data, notable deviations in the extent of error reduction emerge. These differences can primarily be attributed to discrepancies between the motor models used in the simulations and those encountered in practice, as well as variations in operational conditions and parameter tuning. Nevertheless, the trend of error mitigation remains consistent across both frameworks, highlighting the effectiveness and practicality of the proposed approach through this reciprocal validation process.

7. Conclusions

This paper focuses on macro–micro composite motion stages in high-end equipment, such as chip packaging equipment and ultra-precision laser cutting. It specifically investigates the nonlinear friction problem of the large-stroke macro stage, addressing the challenge of simultaneously improving point-to-point positioning and trajectory tracking control performance, which is difficult for existing controllers. A composite controller structure is proposed based on the dynamic modeling of the macro stage and a reduced-order model parameter identification. This controller effectively reduces overshoot and settling time during the macro stage positioning phase through a tracking differentiator and gain-scheduled PID control. Additionally, it significantly diminishes tracking error in the macro stage through a plug-in repetitive controller. The effectiveness of the proposed CCA method in point-to-point response and trajectory tracking control is validated through simulation analysis and actual experiments on the macro–micro stage. In comparison with

the method without CCA, the proposed CCA method reduces settling time and overshoot by 27.3% and 93.2%, respectively, in the point-to-point response with a 10 mm stroke, 0.1 m/s velocity, and 10 m/s² acceleration. In sinusoidal trajectory tracking with a 10 mm amplitude and 2 Hz frequency, the STD tracking error is reduced by 82.73%. Therefore, the proposed composite controller provides an effective control strategy for simultaneously improving the macro stage's point-to-point positioning and trajectory-tracking performance. In future research, we will further consider nanoscale positioning accuracy for micro stages to enhance the control performance of the macro stage.

Author Contributions: Writing—original draft and methodology, Z.Z.; funding acquisition, supervision, and project administration, J.G.; investigation, L.Z. All authors have read and agreed to the published version of the manuscript.

Funding: This research received support from the National Natural Science Foundation of China (Grant No. 52075106 and No. 52375488), the Ministry of Industry and Information Technology of China (Grant No. TC220A04A-206), the R&D project of Guangdong Province (Grant No. 20220166003240), and the Natural Science Foundation of Guangdong Province (Grant No. 2024A1515030003).

Data Availability Statement: Data are contained within the article.

Conflicts of Interest: The authors declare no conflicts of interest.

References

1. Salton, A.T.; Fu, M.Y.; Flores, J.V.; Zheng, J.C. High Precision Over Long Range: A Macro–Micro Approach to Quantized Positioning Systems. *IEEE Trans. Contr. Syst.* **2021**, *29*, 2406–2415. [CrossRef]
2. Zhang, Z.J.; Luo, M.Z.; Duan, J.A.; Kou, B.Q. Design and Analysis of a Novel Frequency Modulation Secondary for High-Speed Permanent Magnet Linear Synchronous Motor. *IEEE ASME Trans. Mech.* **2022**, *27*, 790–799. [CrossRef]
3. Dong, Z.B.; Sun, Z.; Sun, H.; Wang, W.J.; Mei, X.S. A Novel Control Method for Permanent Magnet Synchronous Linear Motor Based on Model Predictive Control and Extended State Observer. *Actuators* **2024**, *13*, 34. [CrossRef]
4. Mehrabi, H.; Hamedi, M.; Aminzahed, I. A novel design and fabrication of a micro-gripper for manipulation of micro-scale parts actuated by a bending piezoelectric. *Microsyst. Technol.* **2020**, *26*, 1563–1571. [CrossRef]
5. Ma, X.F.; Liu, Y.X.; Deng, J.; Gao, X.; Cheng, J.F. A compact inchworm piezoelectric actuator with high speed: Design, modeling, and experimental evaluation. *Mech. Syst. Signal Pr.* **2023**, *184*, 109704. [CrossRef]
6. Chen, X.Y.; Liu, H.W.; Wen, G.H.; Liu, Y.; Cao, J.D.; Qiu, J.L. Adaptive Neural Preassigned-Time Control for Macro–Micro Composite Positioning Stage with Displacement Constraints. *IEEE Trans. Ind Inf.* **2024**, *20*, 1103–1112. [CrossRef]
7. Salton, A.T.; Chen, Z.Y.; Zheng, J.C.; Fu, M.Y. Constrained optimal preview control of dual-stage actuators. *IEEE ASME T Mech.* **2016**, *21*, 1179–1184. [CrossRef]
8. Tian, C.; Yan, P. Data-driven iterative tuning based active disturbance rejection control for piezoelectric nano-positioners. *Mechatronics* **2020**, *65*, 102321. [CrossRef]
9. Xu, Q.S. New Flexure Parallel-Kinematic Micropositioning System With Large Workspace. *IEEE Trans. Robot.* **2012**, *28*, 478–491. [CrossRef]
10. Zhan, B.Y.; Zhang, L.Y.; Liu, Y.C.; Gao, J. Model predictive and compensated ADRC for permanent magnet synchronous linear motors. *ISA Trans.* **2023**, *136*, 605–621. [CrossRef]
11. Yang, X.J.; Liu, H.; Yang, Q.Y.; Zhao, W.H. A novel precision evaluation and analysis method for the direct driven high-speed feed system. *Mech Syst Signal Pr.* **2019**, *121*, 689–710. [CrossRef]
12. Jiao, Z.X.; Cao, Y.; Yan, L.; Li, X.L.; Zhang, L.; Li, Y. Advancing Motivation Feedforward Control of Permanent Magnetic Linear Oscillating Synchronous Motor for High Tracking Precision. *Actuators* **2021**, *10*, 128. [CrossRef]
13. Chen, J.S.; Chen, K.C.; Lai, Z.C.; Huang, Y.K. Friction characterization and compensation of a linear-motor rolling-guide stage. *Int. J. Mach. Tool Manuf.* **2003**, *43*, 905–915. [CrossRef]
14. Wu, J.; Wang, J.S.; Wang, L.P.; Li, T.M. Dynamics and control of a planar 3-DOF parallel manipulator with actuation redundancy. *Mech. Mach. Theory.* **2009**, *44*, 835–849. [CrossRef]
15. Li, Y.B.; Wang, L.; Chen, B.; Wang, Z.S.; Sun, P.; Zheng, H.; Xu, T.T.; Qin, S.Y. Optimization of dynamic load distribution of a serial-parallel hybrid humanoid arm. *Mech. Mach. Theory.* **2020**, *149*, 103792. [CrossRef]
16. Wang, Z.; Hu, C.; Zhu, Y. Accelerated iteration algorithm based contouring error estimation for multiaxis motion control. *IEEE-ASME Trans. Mech.* **2022**, *27*, 452–462. [CrossRef]
17. Shin, H.B.; Park, J.G. Anti-Windup PID Controller with Integral State Predictor for Variable-Speed Motor Drives. *IEEE Trans. Ind. Electron.* **2012**, *59*, 1509–1516. [CrossRef]
18. Wu, J.H.; Xiong, Z.H.; Lee, K.M.; Ding, H. High-Acceleration Precision Point-to-Point Motion Control With Look-Ahead Properties. *IEEE Trans. Ind. Electron.* **2011**, *58*, 4343–4352.

19. Tang, H.; Gao, J.; Chen, X.; Yu, K.M.; To, S.; He, Y.B.; Chen, X.; Zheng, Z.H.; He, S.F.; Chen, C.B.; et al. Development and Repetitive-Compensated PID Control of a Nanopositioning Stage with Large-Stroke and Decoupling Property. *IEEE Trans. Ind. Electron.* **2018**, *65*, 3995–4005. [CrossRef]
20. Zhang, L.Y.; Gao, J.; Chen, X. A rapid dynamic positioning method for settling time reduction through a macro-micro composite stage with high positioning accuracy. *IEEE Trans. Ind. Electron.* **2018**, *65*, 4849–4860. [CrossRef]
21. Song, J.C.; Dong, F.; Zhao, J.W.; Wang, H.; He, Z.Y.; Wang, L.J. An Efficient Multiobjective Design Optimization Method for a PMSLM Based on an Extreme Learning Machine. *IEEE Trans. Ind. Electron.* **2019**, *66*, 1001–1011. [CrossRef]
22. Delibas, B.; Koc, B. A Method to Realize Low Velocity Movability and Eliminate Friction Induced Noise in Piezoelectric Ultrasonic Motors. *IEEE ASME Trans. Mech.* **2020**, *25*, 2677–2687. [CrossRef]
23. Zheng, M.; Zhou, S.Y.; Tomizuka, M. A Design Methodology for Disturbance Observer with Application to Precision Motion Control: An H-infinity Based Approach. In Proceedings of the IEEE 2017 American Control Conference (ACC), Seattle, WA, USA, 24–26 May 2017; pp. 3524–3529.
24. Radac, M.B.; Precup, R.E.; Petriu, E.M. Model-Free Primitive-Based Iterative Learning Control Approach to Trajectory Tracking of MIMO Systems With Experimental Validation. *IEEE Trans. Neur. Net. Lear.* **2015**, *26*, 2925–2938. [CrossRef] [PubMed]
25. Cui, J.; Zhao, F.; Chu, Z. Experiment on trajectory tracking control of high precise positioning system based on iterative learning controller with wavelet filtering. *Mechatronics* **2015**, *32*, 88–95. [CrossRef]
26. Liu, P.B.; Yan, P.; Hitay, O. Design and trajectory tracking control of a piezoelectric nano-manipulator with actuator saturations. *Mech. Syst. Signal Pr.* **2018**, *111*, 529–544. [CrossRef]
27. Yang, M.J.; Gu, G.Y.; Zhu, L.M. High-bandwidth tracking control of piezo-actuated nanopositioning stages using closed-loop input shaper. *Mechatronics* **2014**, *24*, 724–733. [CrossRef]
28. Wang, Y.W.; Zhang, W.A.; Yu, L. GESO-Based Position Synchronization Control of Networked Multi-Axis Motion System. *IEEE Trans. Ind. Inf.* **2020**, *16*, 248–257. [CrossRef]
29. Li, C.X.; Gu, G.Y.; Zhu, L.M.; Su, C.Y. Odd-harmonic repetitive control for high-speed raster scanning of piezo-actuated nanopositioning stages with hysteresis nonlinearity. *Sens. Actuat. A Phys.* **2016**, *244*, 95–105. [CrossRef]
30. Aljanaideh, M.; Rakotondrabe, M.; Aidarabsah, I.; Aljanaideh, O. Internal model-based feedback control design for inversion-free feedforward rate-dependent hysteresis compensation of piezoelectric cantilever actuator. *Control Eng. Pract.* **2018**, *72*, 29–41. [CrossRef]
31. Tian, J.; Yuan, L.; Xiao, W.D.; Ran, T.; Zhang, J.B.; Li, H. Optimal robust control with cooperative game theory for lower limb exoskeleton robot. *Nonlinear Dynam.* **2022**, *108*, 1283–1303. [CrossRef]
32. Wu, Z.G.; Chen, M.; Ping, M.H.; Li, H.; Zhang, Q.; Xiong, X.Z.; Mi, H.Y.; Li, Z.X.; Li, Y.M. Tracking control of PZT-Driven compliant precision positioning micromanipulator. *IEEE Access* **2020**, *8*, 126477–126487. [CrossRef]
33. Lin, C.; Zheng, S.; Li, P.Y.; Jiang, M.D. Kinetostatic analysis of 6-DOF compliant platform with a multi-stage condensed modeling method. *Microsyst. Technol.* **2021**, *27*, 2153–2166. [CrossRef]
34. Kim, K.; Choi, Y.M.; Nam, B.U.; Lee, M.G. Dual Servo Stage Without Mechanical Coupling for Process of Manufacture and Inspection of Flat Panel Displays Via Modular Design Approach. *Int. J. Precis. Eng. Man.* **2012**, *13*, 407–412. [CrossRef]
35. Zhang, J.D.; Gao, J.; Zhang, L.Y.; Luo, Y.H.; Chen, X.; Chen, X.; He, Y.B. Novel Dynamic Microactuation Method for Tracking-Error Reduction of Permanent Magnet Linear Synchronous Motors. *IEEE Trans. Ind. Electron.* **2022**, *69*, 9165–9175. [CrossRef]
36. Feng, C.L.; Chen, W.D.; Shao, M.Q.; Ni, S.H. Trajectory Tracking and Adaptive Fuzzy Vibration Control of Multilink Space Manipulators with Experimental Validation. *Actuators* **2023**, *12*, 138. [CrossRef]
37. Liu, Y.C.; Gao, J.; Zhong, Y.B.; Zhang, L.Y. Extended State Observer-Based IMC-PID Tracking Control of PMLSM Servo Systems. *IEEE Access* **2020**, *9*, 49036–49046. [CrossRef]

Disclaimer/Publisher's Note: The statements, opinions and data contained in all publications are solely those of the individual author(s) and contributor(s) and not of MDPI and/or the editor(s). MDPI and/or the editor(s) disclaim responsibility for any injury to people or property resulting from any ideas, methods, instructions or products referred to in the content.